

Supporting Information

In-Situ processed gold nanoparticle embedded TiO₂ nanofibers for efficient plasmonic perovskite solar cells exceeding 14% conversion efficiency

*Sawanta S. Mali, Chang Su Shim, Chang Kook Hong**

*Polymer Energy Materials Laboratory, School of Applied Chemical Engineering, Chonnam National University, Gwangju, 500-757 (South Korea).

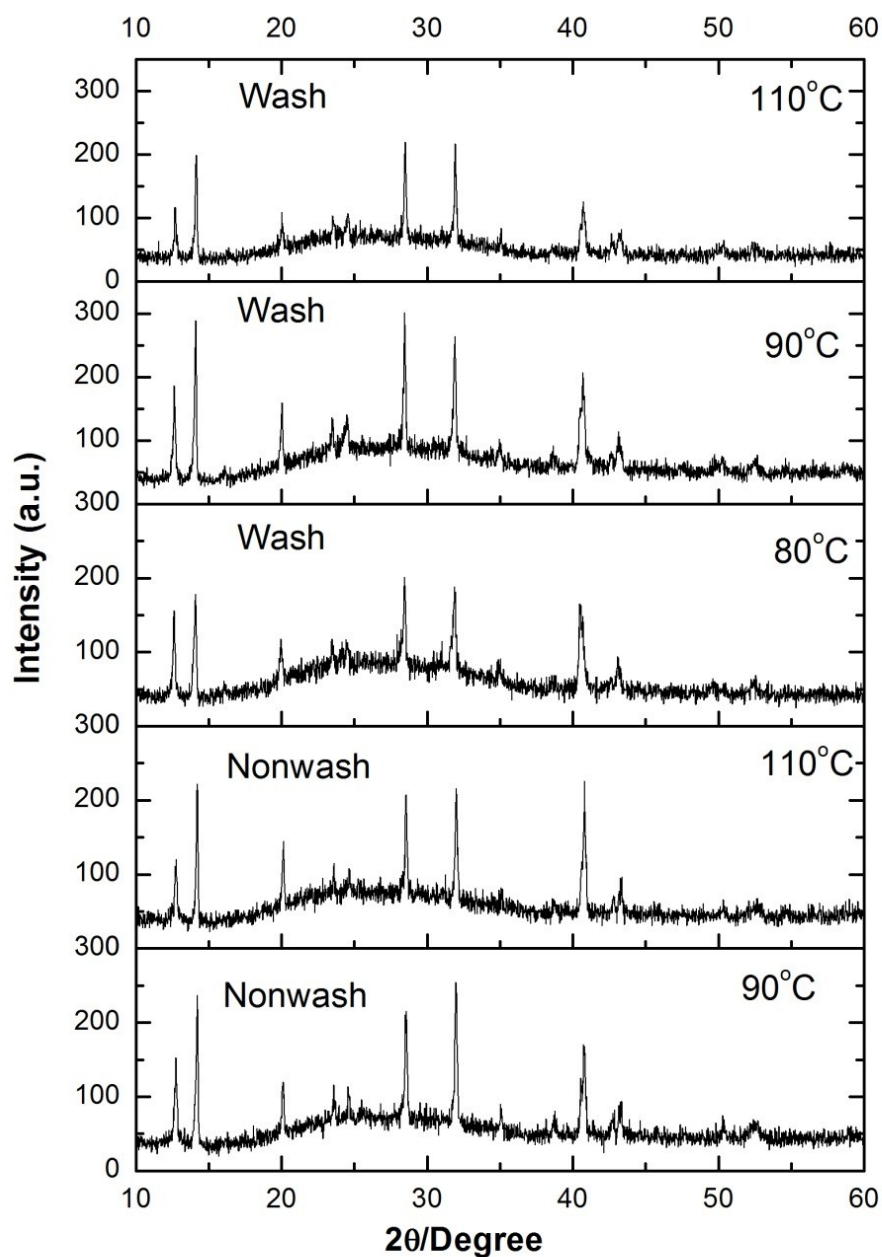
S1 Characterizations:

The top-surface and cross-sectional images were recorded by a field emission scanning electron microscope (FESEM; S-4700, Hitachi). Transmission electron microscopy (TEM) micrographs, selected area electron diffraction (SAED) pattern and high-resolution transmission electron microscopy (HRTEM) images were obtained by TECNAI F20 Philips operated at 200 KV. The TEM sample was prepared by drop casting of ethanolic dispersion of sample onto a carbon coated Cu grid. X-ray diffraction (XRD) measurements were carried out using a D/MAX Ultima III XRD spectrometer (Rigaku, Japan) with Cu K line of 1.5410 Å. The elemental information regarding the deposited samples were analyzed using an X-ray photoelectron spectrometer (XPS) (VG Multilab 2000-Thermo Scientific, USA, K-Alpha) with a multi-channel detector, which can endure high photonic energies from 0.1 to 3 keV.

The open circuit voltage decay (OCVD) measurements were obtained Iviumstat workstation (Ivium Technologies B.V., Eindhoven, The Netherlands). The cells were illuminated using a solar simulator at AM 1.5 G for 10 s, where the light intensity was adjusted with an NREL-calibrated Si solar cell with a KG-5 filter to 1 sun intensity (100 mW cm⁻²). OCVD method was performed on a photovoltaic device by abruptly turning off the illumination and recording the Voc decay. The IPCE spectra were measured as a function of wavelength from 300 to 1100 nm on the basis of a Spectral Products DK240 monochromator. Impedance spectroscopy (IS) was conducted using Iviumstat (Ivium Technologies B.V., Eindhoven, the Netherlands) at an open-circuit potential at frequencies ranging from 10⁻¹ to 10⁵ Hz with an AC amplitude of 10 mV. The amplitude of the modulation voltage was 10 mV. Z-view2.8d (Scribner Associates) was used to fit the EIS spectra to the equivalent circuit based on the transmission line model. The DC bias potential was applied in 0.05V step intervals. Photoluminescence measurements were carried out on a PL mapper (Accent Opt. Tech. UK, Model:RPM2000, 532nm ND-YAG laser excitation). Time-resolved

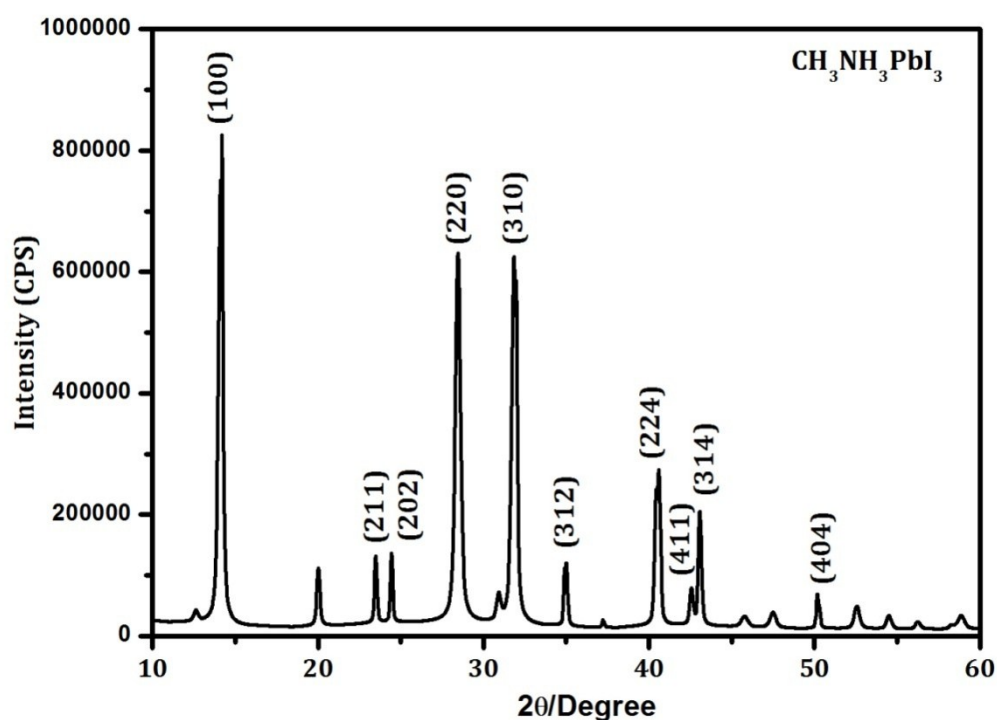
photoluminescence (PL) decay transients were measured at $750\pm 20\text{nm}$ using excitation with a 470nm light pulse at a frequency of 5MHz from the Spectrophotometer F-7000. Optical absorption measurements were carried out on a UV-vis spectrophotometer (Varian, CARY, 300 Conc.) in the $280\text{-}900\text{ nm}$ wavelength range.

Figure S1 (a) Optimization of phase pure $(\text{CH}_3\text{NH}_3)\text{PbI}_3$. XRD patterns of synthesized $(\text{CH}_3\text{NH}_3)\text{PbI}_3$ at different conditions.



We have optimized our perovskite synthesis recipe with respect to washing MAI with diethyl ether, recrystallize process and drying temperature. Our results indicate that the $\text{CH}_3\text{NH}_3\text{PbI}_3$ dried at 90°C shows good photo-conversion efficiency. Double wash MAI was used for perovskite synthesis.

Figure S1(b) XRD pattern of optimized $\text{CH}_3\text{NH}_3\text{PbI}_3$ sample deposited on glass substrate. The MAI was prepared and recrystallized three times using diethyl ether.



The XRD results reveal $\text{CH}_3\text{NH}_3\text{PbI}_3$ characteristic peaks at 14.36, 28.61, 32.081, and 40.648 corresponding to the (110), (220), (310) and (224) planes of $\text{CH}_3\text{NH}_3\text{PbI}_3$, respectively, as shown in Figure S1(b). Our calculated lattice parameters for $\text{CH}_3\text{NH}_3\text{PbI}_3$ with a tetragonal unit cell are $a=b=8.879\text{\AA}$ and $c=12.558\text{\AA}$ which is in agreement with previous reports $a=b=8.883\text{\AA}$ and $c=12.677\text{\AA}$ [1, 2, 3].

References:

- [1] Kawamura Y., Masghiyama H. & Hasebe K., Structural study on cubic-tetragonal transition of $\text{CH}_3\text{NH}_3\text{PbI}_3$, *J. Phys. Soc. Jpn*, 71, 1694-1697 (2002)
- [2] Poglitsch A. & Weber D., Dynamic disorder in methylammonium trihalogenoplumbates(II) observed by millimeter-wave spectroscopy, *J. Chem. Phys.*, 87, 6373-6377 (1987).
- [3] Supasai T., Rujisamphan N., Ullrich K., Chemseddine A. & Dittrich Th., Formation of a passivating $\text{CH}_3\text{NH}_3\text{PbI}_3/\text{PbI}_2$ interface during moderate heating of $\text{CH}_3\text{NH}_3\text{PbI}_3$ layers, *Appl. Phys. Lett.* 103, 183906-3 (2013).

Figure S2 (a) Plan view of STEM micrographs of Au@TiO₂/CH₃NH₃PbI₃ nanofibers and EDS mapping of (b) titanium, (c) oxygen, (d) gold (e) lead and (f) iodine elements.

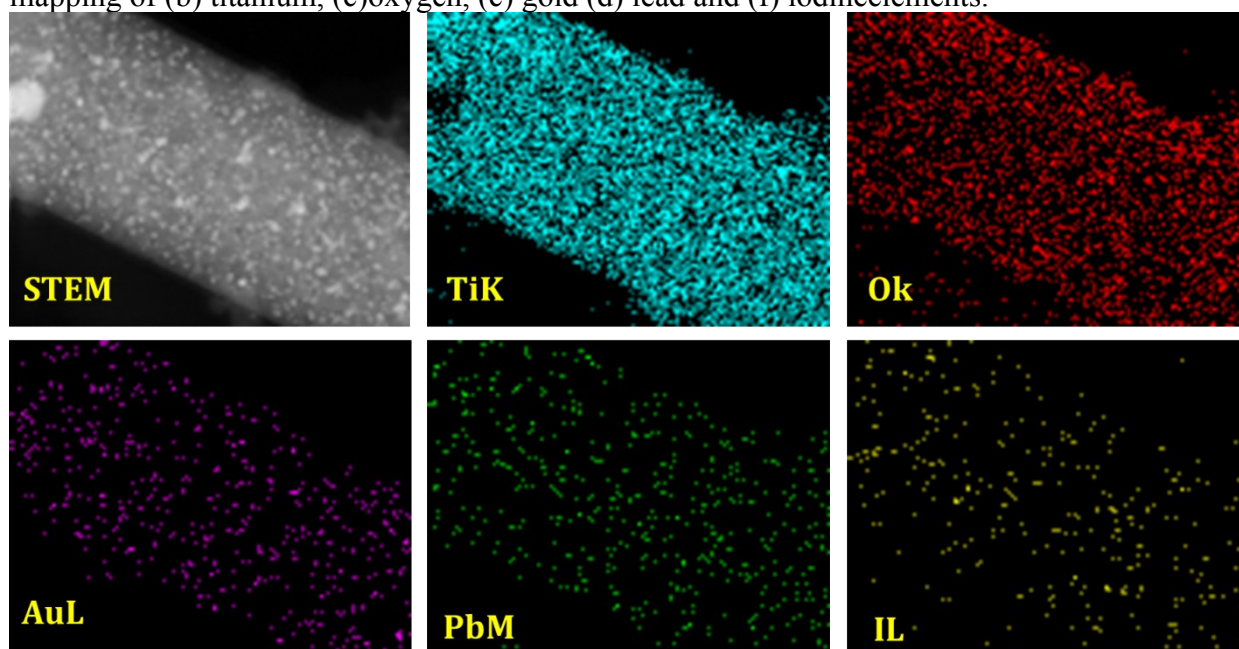


Figure S2 shows high resolution TEM micrographs of TiO₂ nanoparticle loaded with perovskite CH₃NH₃PbI₃ deposited, along with pure CH₃NH₃PbI₃ particles obtained by drying the γ -butyrolactone solution and bare TiO₂ nanoparticles. From STEM image it is clear that, the perovskite CH₃NH₃PbI₃ are homogeneously distributed onto nanoparticulate TiO₂ nanofiber surface. The nanocrystalline CH₃NH₃PbI₃ with ~8-10 nm has been deposited on TiO₂ surface. Moreover, perovskite nanoparticles are well adsorbed on TiO₂ surface as can be seen from the wide view of TEM in inset of Fig. 1(b), which is consistent with the EDS elemental analysis.

Figure S3 Morphological and topological characterization of Au@TiO₂ nanofibers. (a) FESEM image of synthesized Au@TiO₂ nanofibers (b) TEM micrograph of the Au@TiO₂ nanofibers (c) higher magnified image of Au@TiO₂ nanofiber at selected area (d) SAED pattern of Au@TiO₂ sample (e) & (f) higher magnified TEM micrographs of TiO₂ nanofibers and single Au nanoparticle.

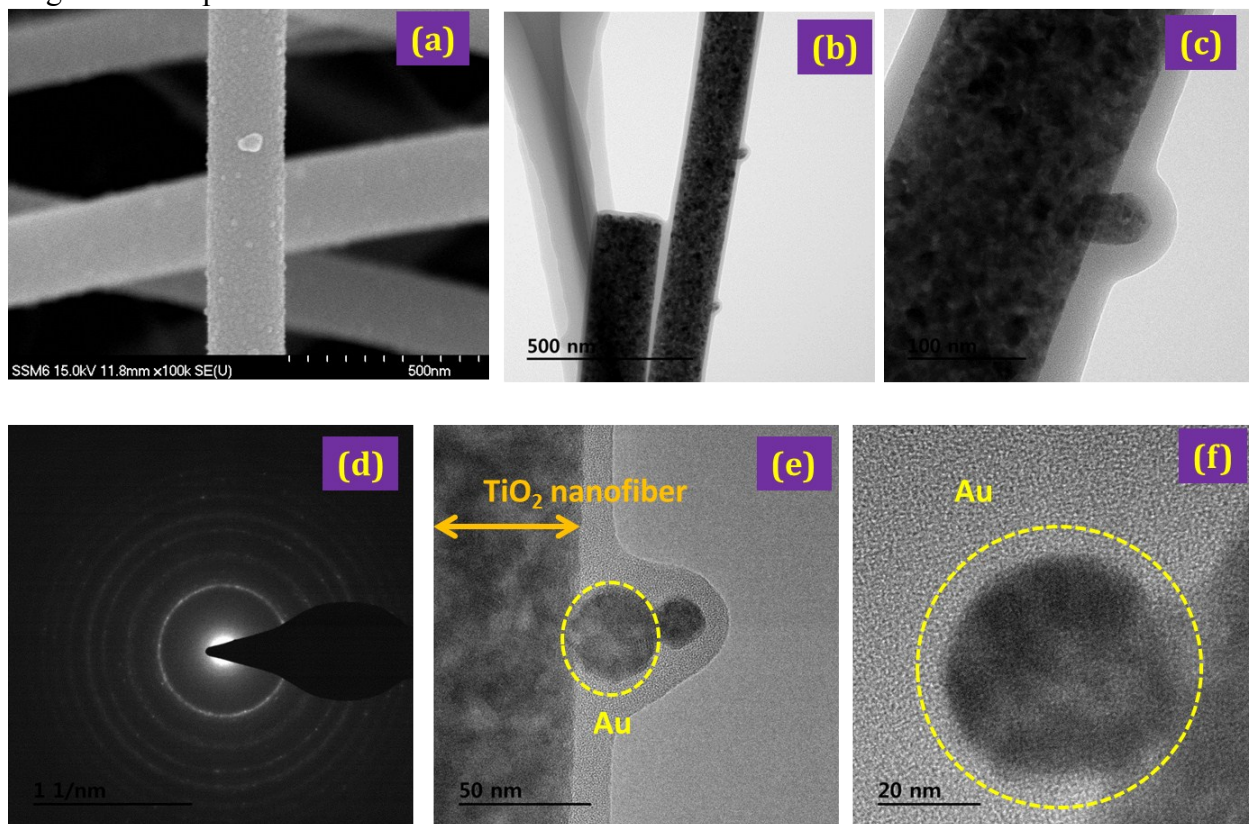


Figure S4 HRTEM characterization of perovskite deposited Au@TiO₂ nanofibers. (a) TEM image of single Au@TiO₂ nanofiber deposited with perovskite (b) (c) and (d) TEM micrograph of the perovskite deposited Au@TiO₂ nanofiber as different magnifications (e) higher magnified image of single Au nanoparticle (e) higher magnified TEM image of selected perovskite area. (g) HRTEM image of selected area showing highly crystalline TiO₂ as well as perovskite.

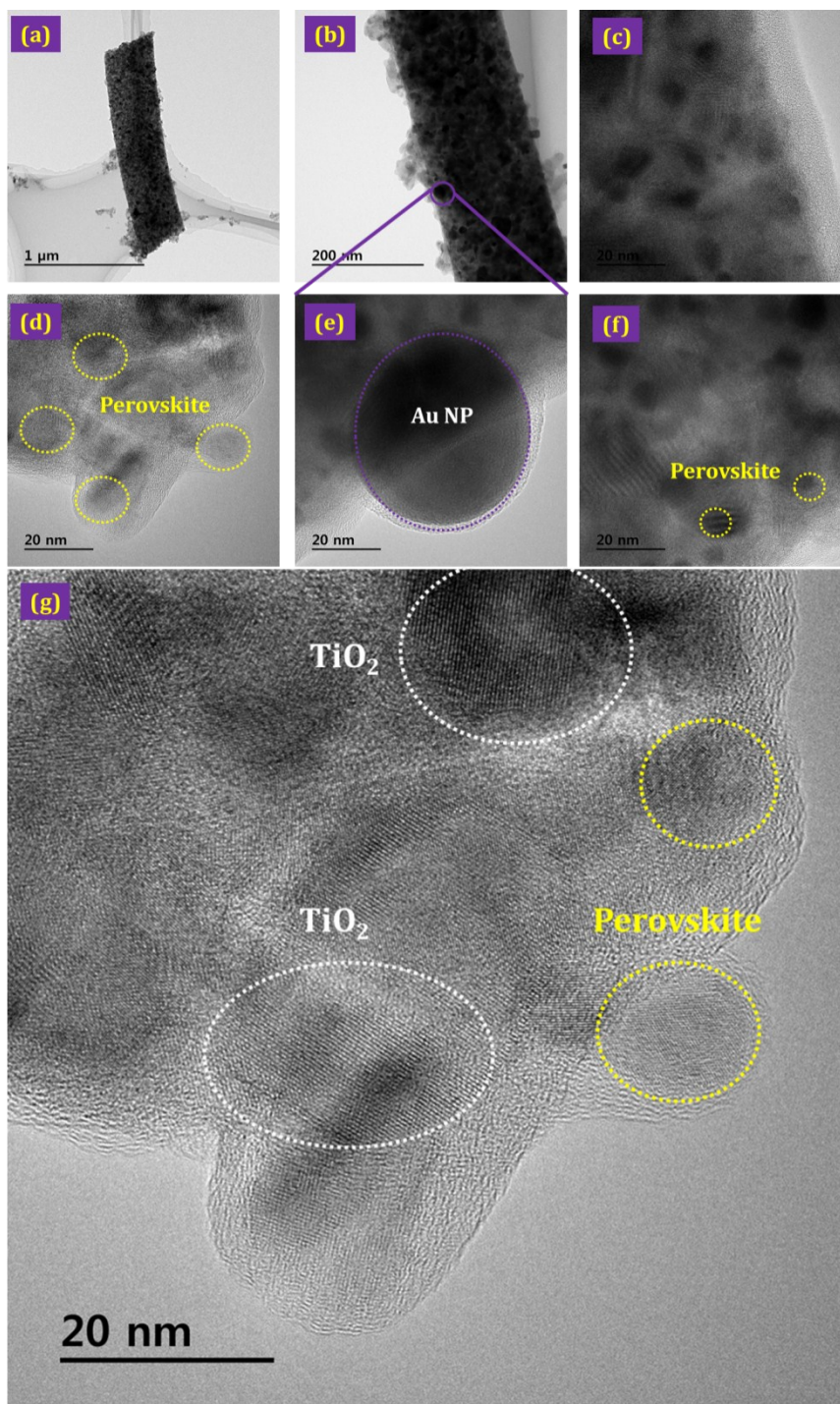


Figure S5 Nitrogen adsorption–desorption isotherms of the TiO₂ and Au@TiO₂ nanofibers.

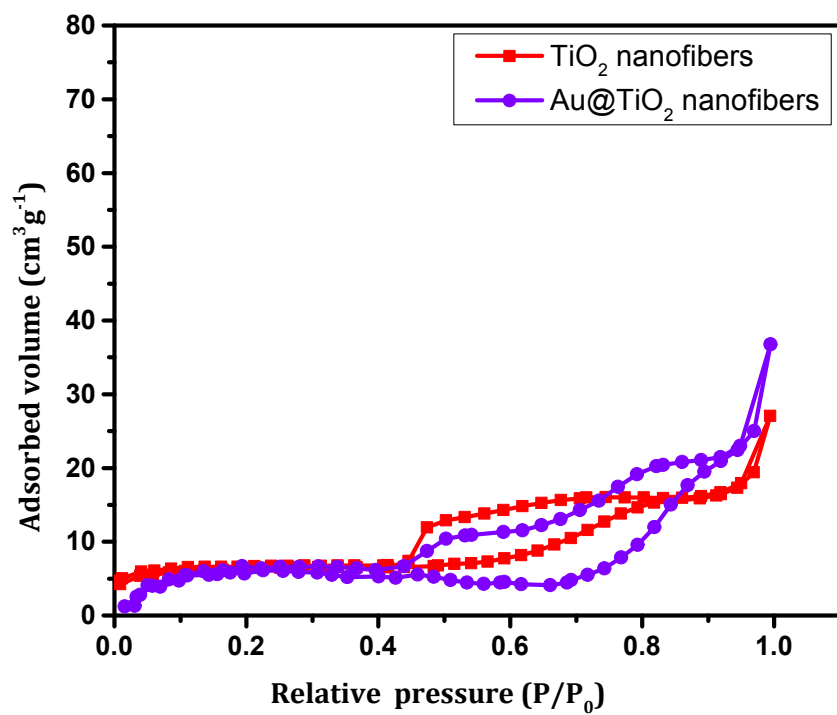


Figure S5 FESEM image of $\text{CH}_3\text{NH}_3\text{PbI}_3$ thin film. Inset photograph shows the prepared fresh $\text{CH}_3\text{NH}_3\text{PbI}_3$ solution in γ -butyrolactone.

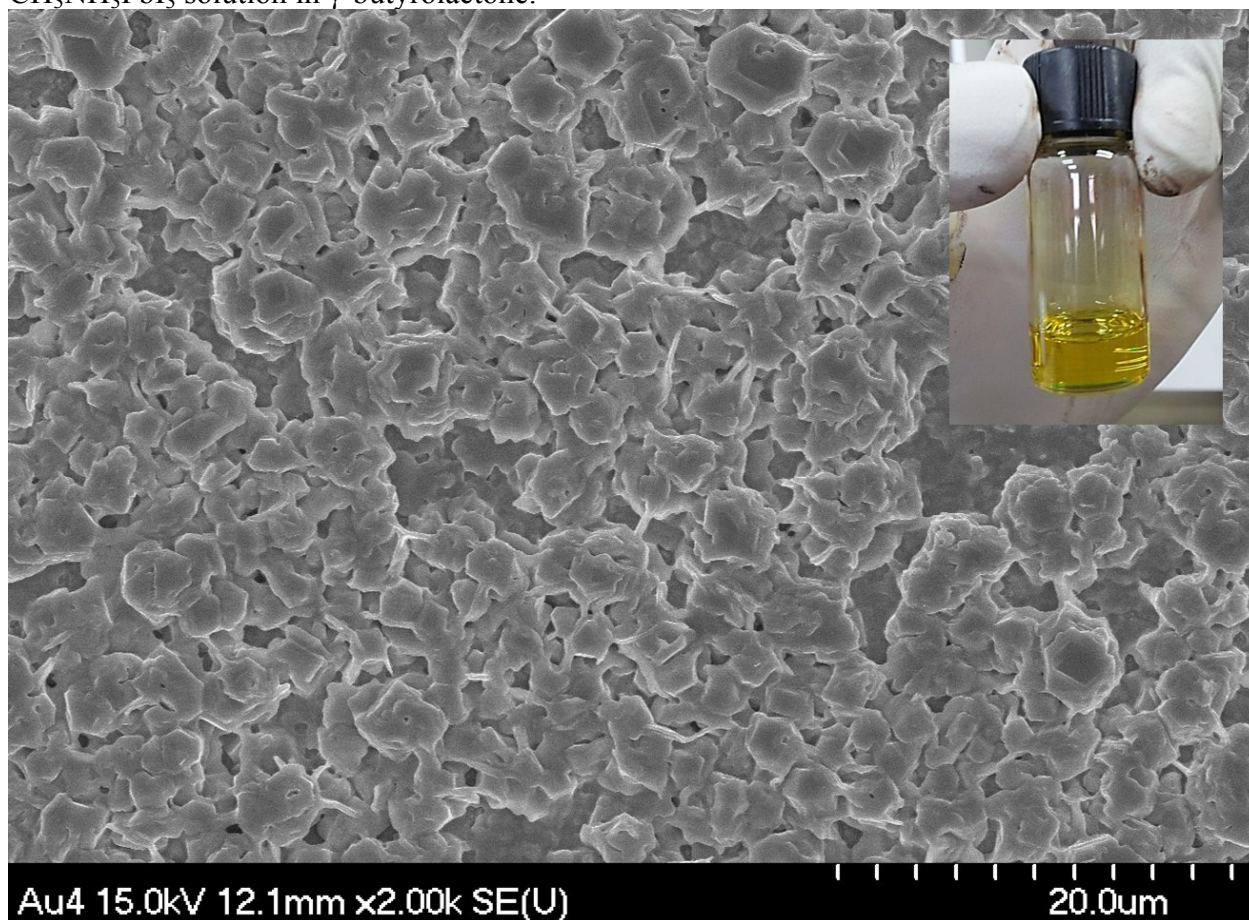


Figure S7 FESEM image of $(\text{CH}_3\text{NH}_3)\text{PbI}_3$ thin film after coating of HTM layer showing islands are covered onto perovskite/Au@TiO₂ surface.

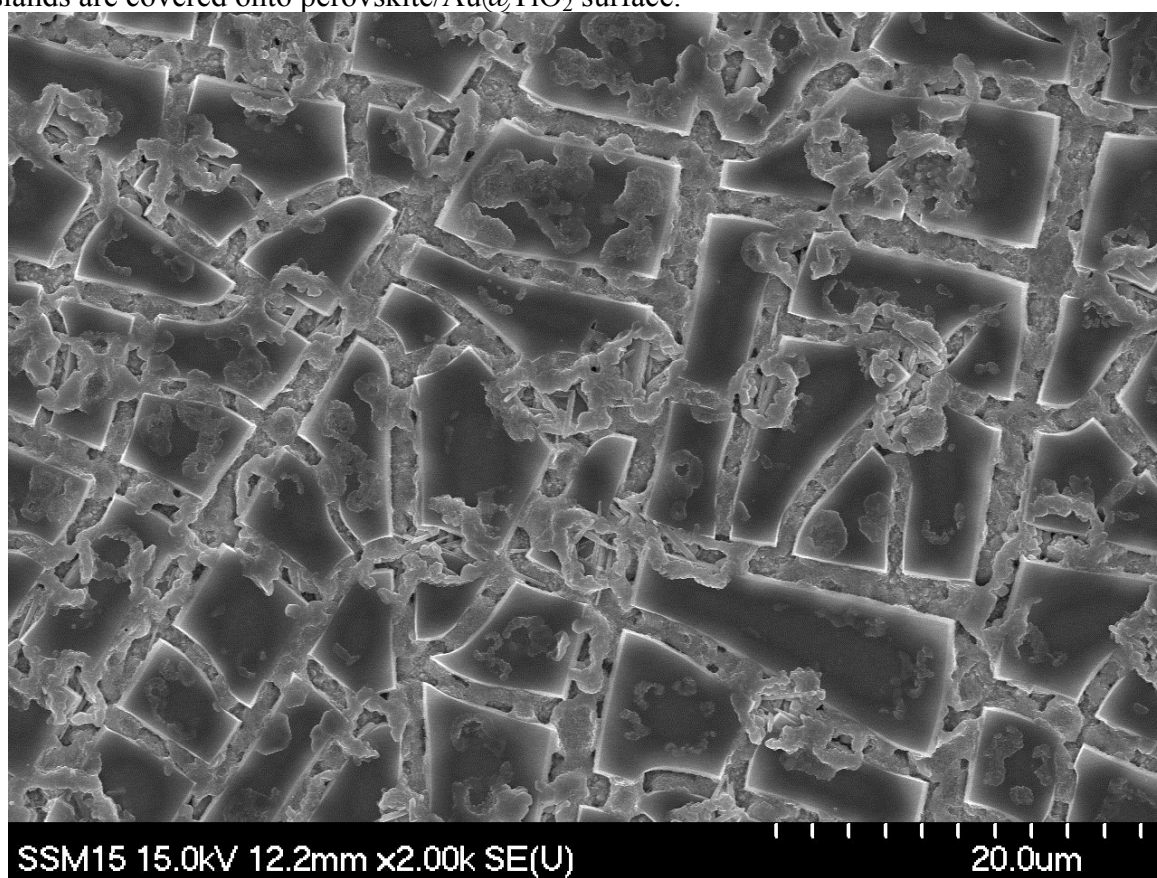


Figure S8. Compositional analysis of Au@TiO₂ nanofiber based perovskite device: (a) Cross-sectional fieldemissionscanning electron micrograph (FESEM) of a fabricated device. (b) Energydispersive x-ray (EDX) spectroscopy analysis with elemental mapping of (c) titanium, (d) lead (e)iodine (f) tin, (h)carbon (Please note that Sn element is present may be due to FTO substrate)

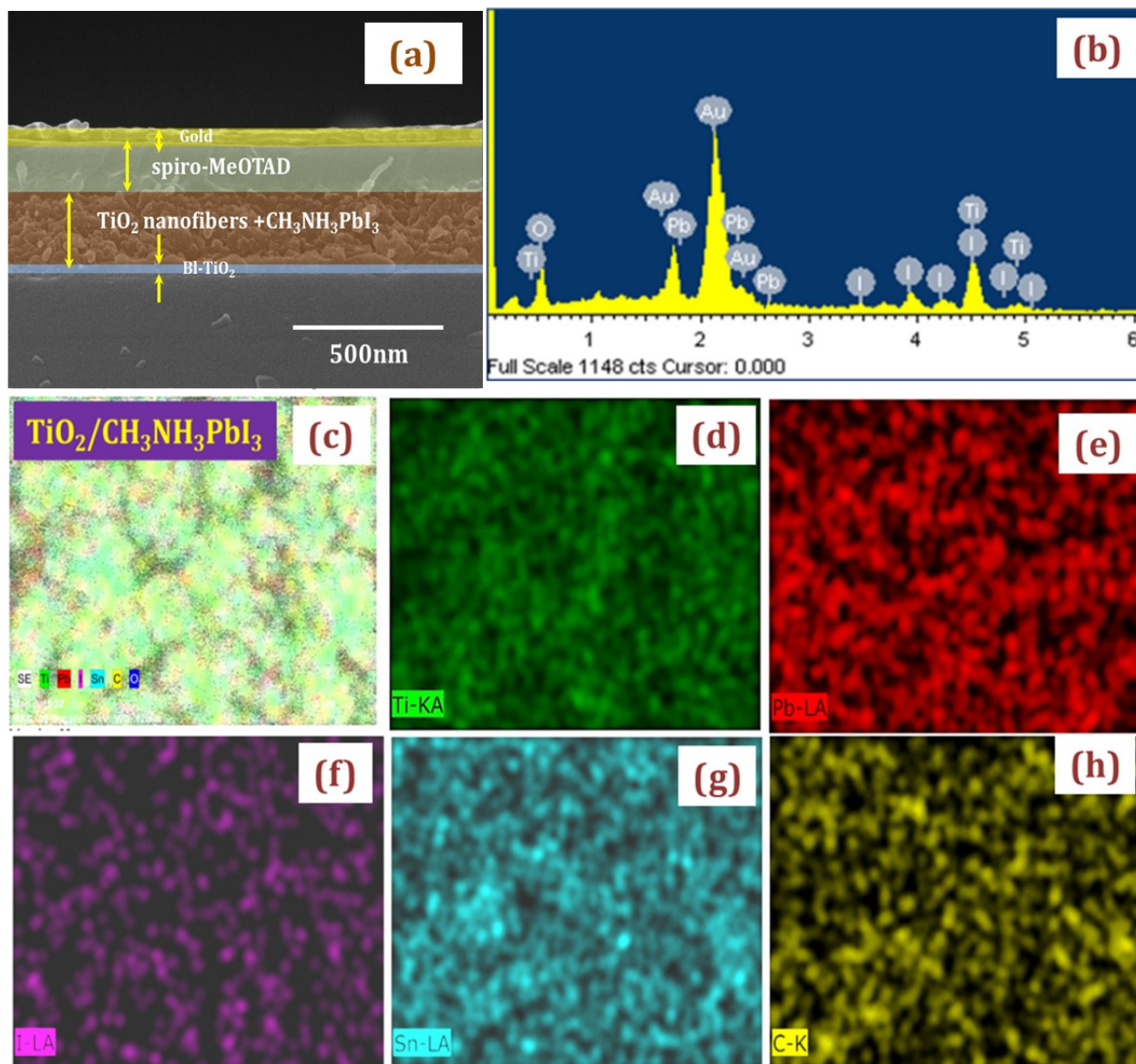


Figure S9 Compositional analysis of perovskite thin films (a) survey spectra of TiO₂ nanofibers/perovskite and Au@TiO₂ nanofibers/perovskite thin films (b) core level spectra of Ti(2p) (c) core level spectra of O(1s) (d) Pb(4f) core level spectra (f) I(3d) core level spectra (g) valence band spectra of CH₃NH₃PbI₃ thin films deposited on TiO₂ and Au@TiO₂ nanofibers. (Pink line perovskite/TiO₂ nanofiber, Violet line perovskite/Au@TiO₂ nanofibers)

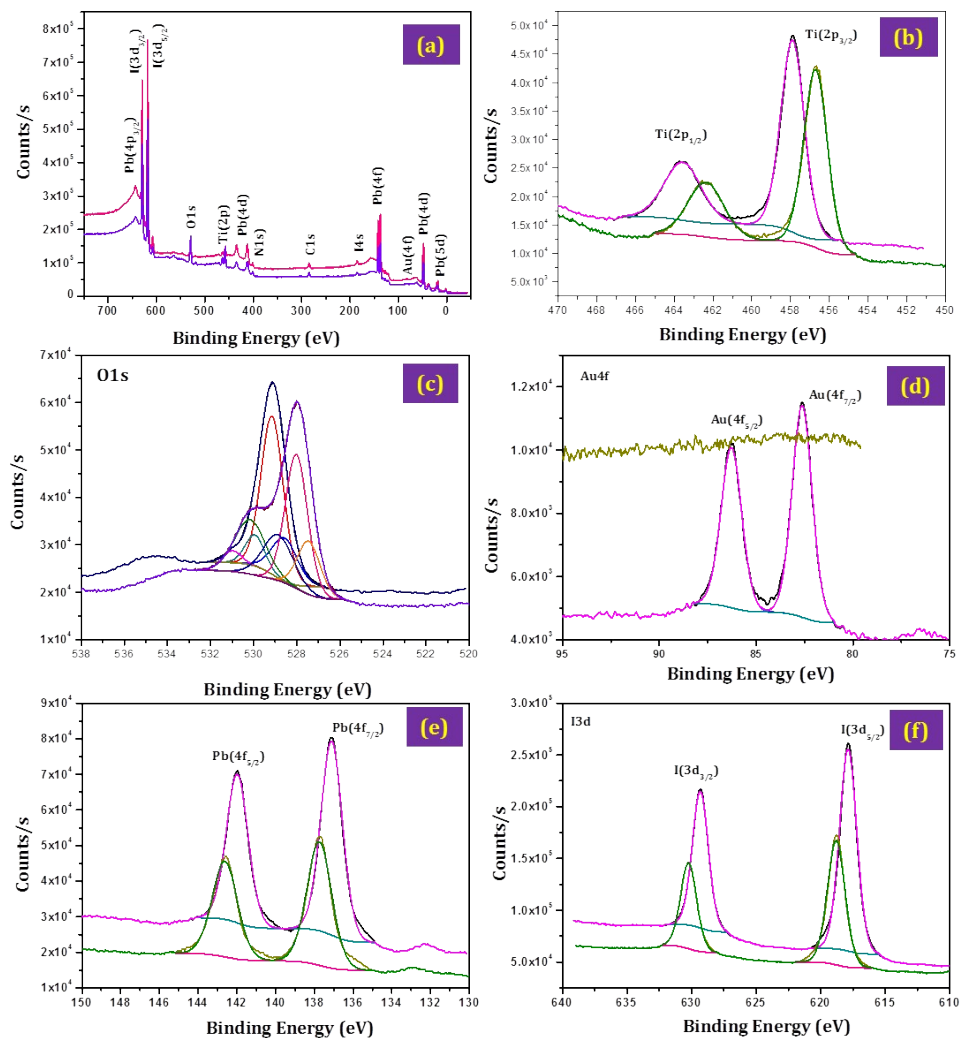


Figure S10 (a) J-V curves measured for perovskite device measured at a simulated AM 1.5G solar irradiation of 100mWcm^{-2} .

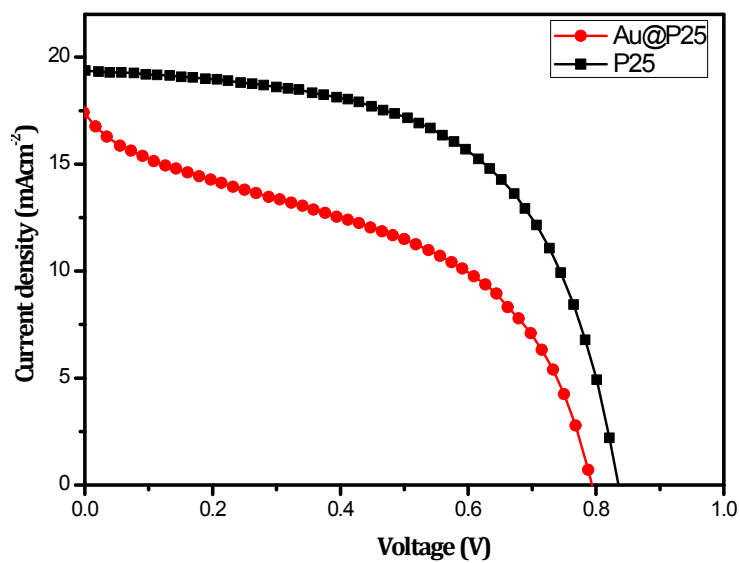


Figure S10 (b) J-V curves measured for perovskite device measured at a simulated AM 1.5G solar irradiation of 100mWcm^{-2} . Nearly 58nm Au NPs initially prepared and then added in mp-TiO₂ paste.

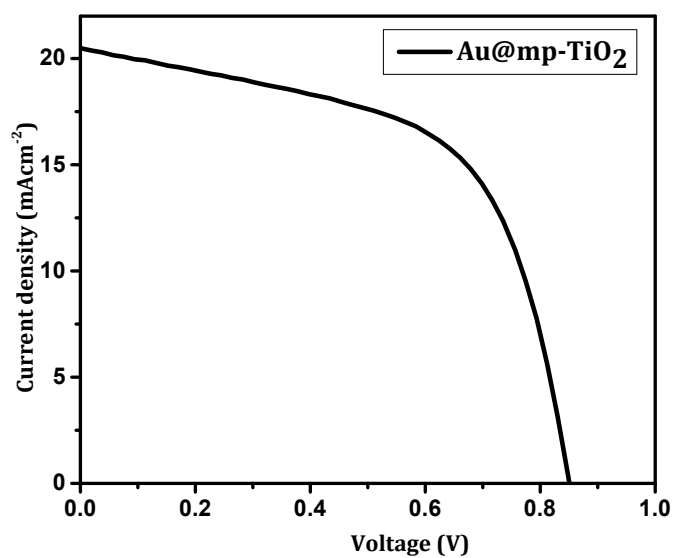


Figure S11 Impedance spectroscopy measurements: Dark current during recorded during IS measurements of TiO₂ nanofibers (pink color) and Au@TiO₂ nanofiber based perovskite devices.

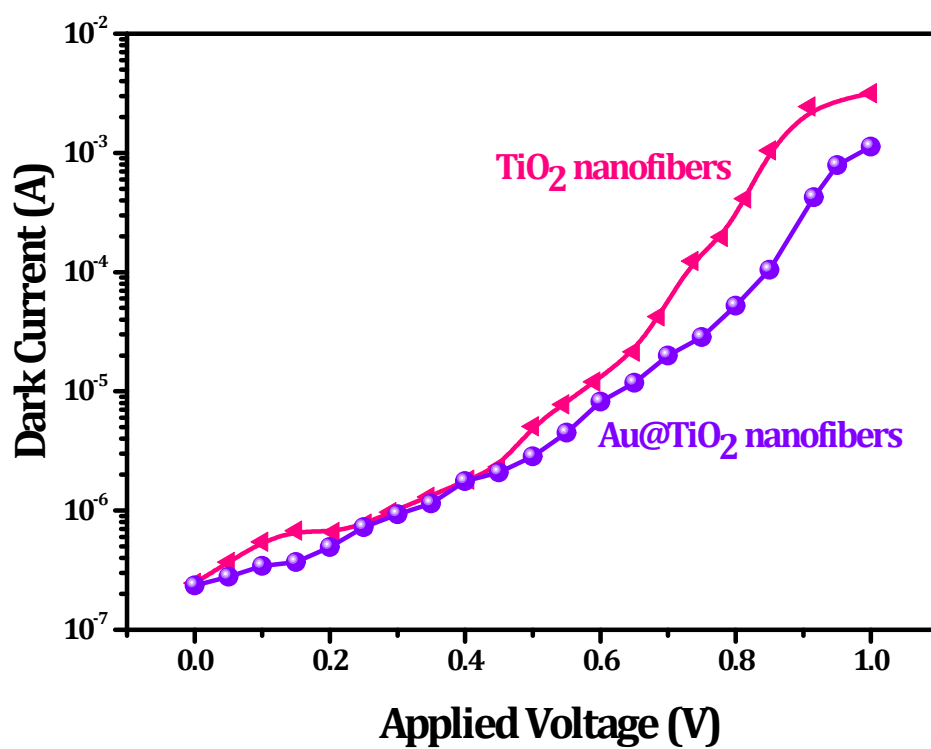


Figure S12 Photograph of synthesized bare TiO₂ nanofibers and Au decorated TiO₂ nanofibers

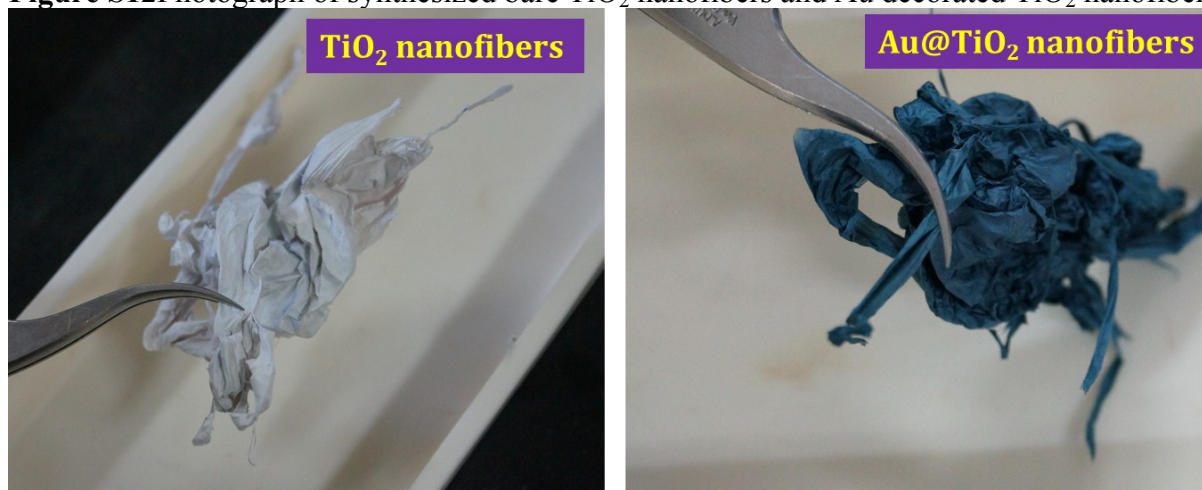


Figure S13. Weight loss as a function of temperature for the as deposited TiO₂ and Au@TiO₂ nanofibers. Thermogravimetric analysis (TGA) was performed at rate of 10°C/min under nitrogen atmosphere (Flow rate: 50ml/min).

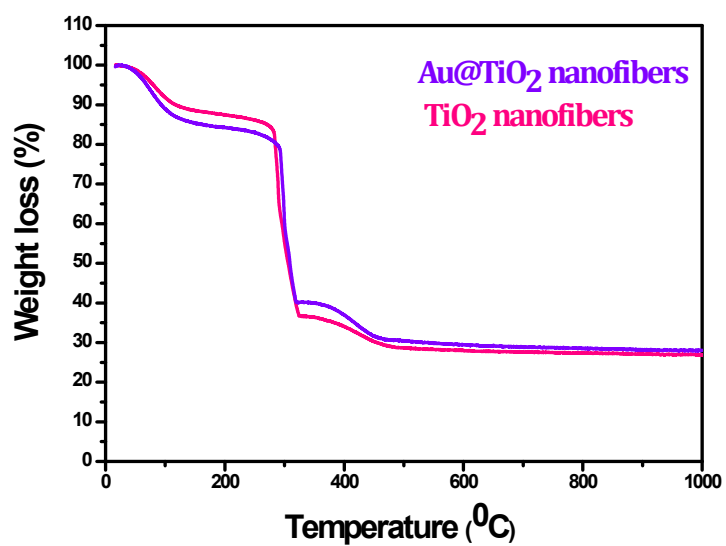


Figure S14 XRD patterns of bare TiO₂ nanofibers and Au@TiO₂ nanofibers.

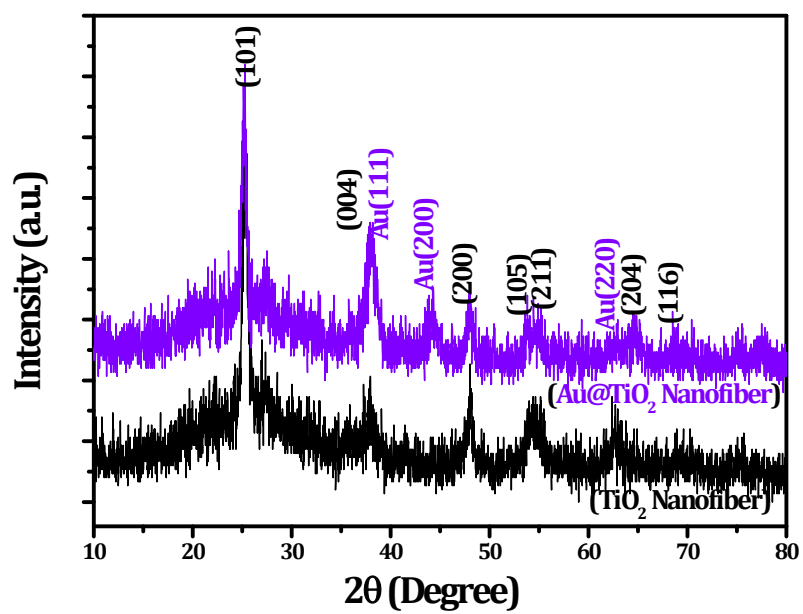


Figure S15 Morphological and topological characterization of TiO₂ nanofiber (a) FESEM image of synthesized TiO₂ nanofibers (b) TEM micrograph of the single nanofiber (c) The higher magnified image (c) HRTEM micrograph of the TiO₂ nanofibers with lattice planes.

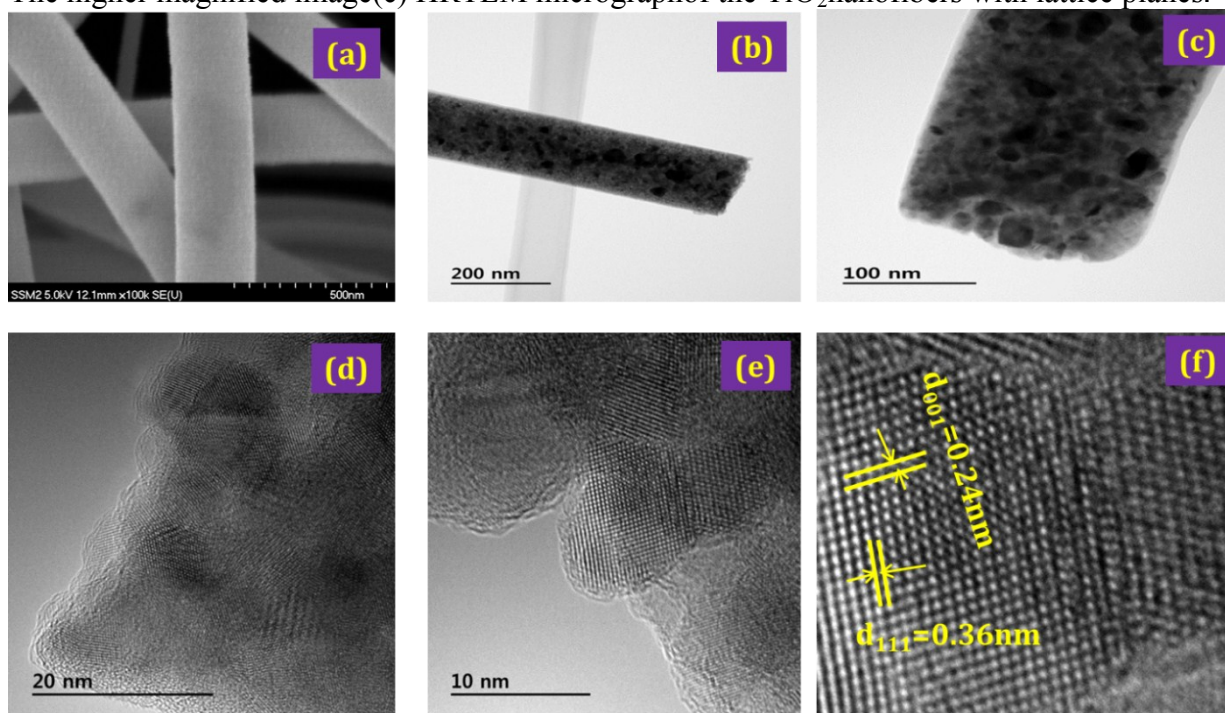


Figure S16 (a) Plan view of SEM micrographs of Au@TiO₂ nanofibers and EDS mapping of (b) titanium, (c) oxygen and (d) gold element mapping.

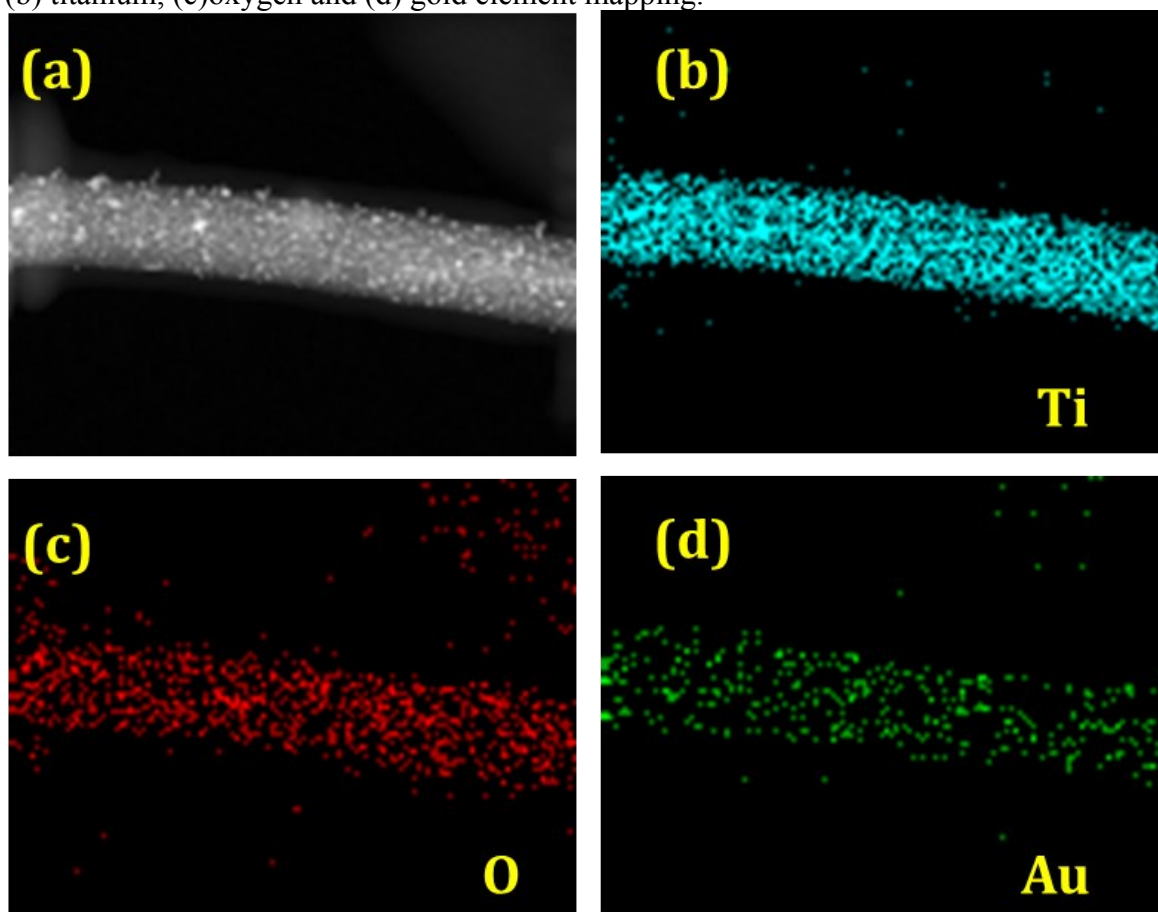


Figure S17. Weight loss as a function of temperature for the mixed MAI and PbI_2 powder. Thermogravimetric analysis (TGA) was performed at rate of $10^\circ\text{C}/\text{min}$ under nitrogen atmosphere (Flow rate: $50\text{ml}/\text{min}$).

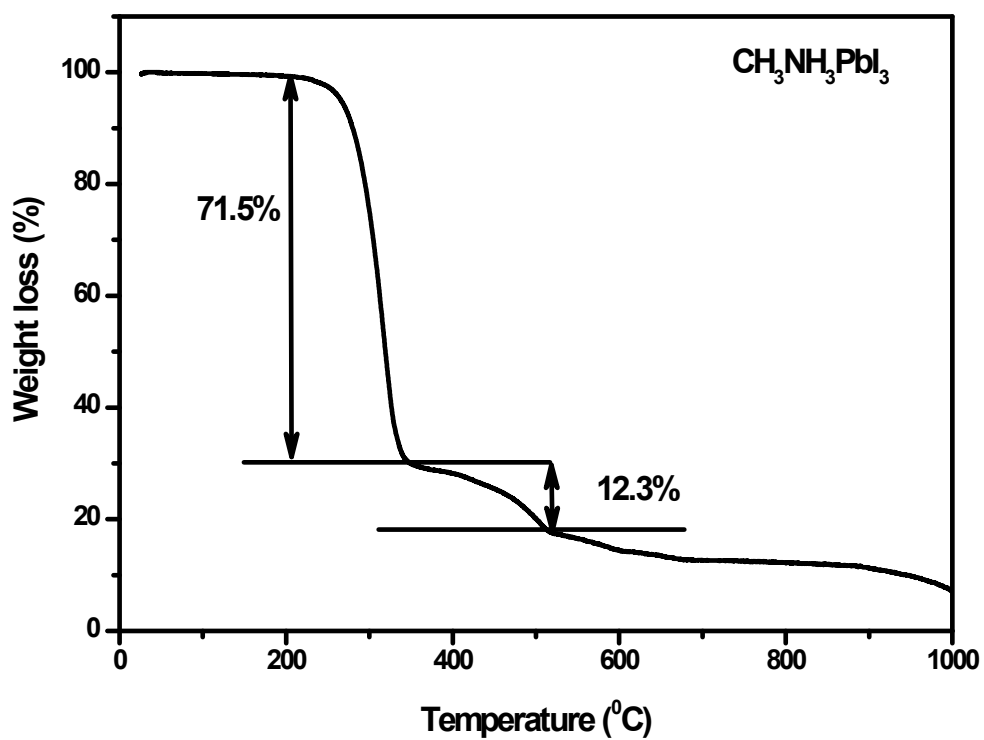


Figure S18 Morphological and topological characterization of mp-TiO₂ based perovskite solar cells. (a) Cross-sectional FESEM image of fabricated perovskite solar cell device. (b) The higher magnified image of perovskite coated mp-TiO₂ of selected area. (c) TEM micrograph of the perovskite (CH₃NH₃)PbI₃ deposited on ms-TiO₂ nanoparticles (d) Highly magnified TEM image of CH₃NH₃PbI₃ coated TiO₂ nanoparticles. (e) SAED pattern of TiO₂ nanoparticles (f) highly magnified TEM image (g) HRTEM image of CH₃NH₃PbI₃ (h) SAED pattern of CH₃NH₃PbI₃.

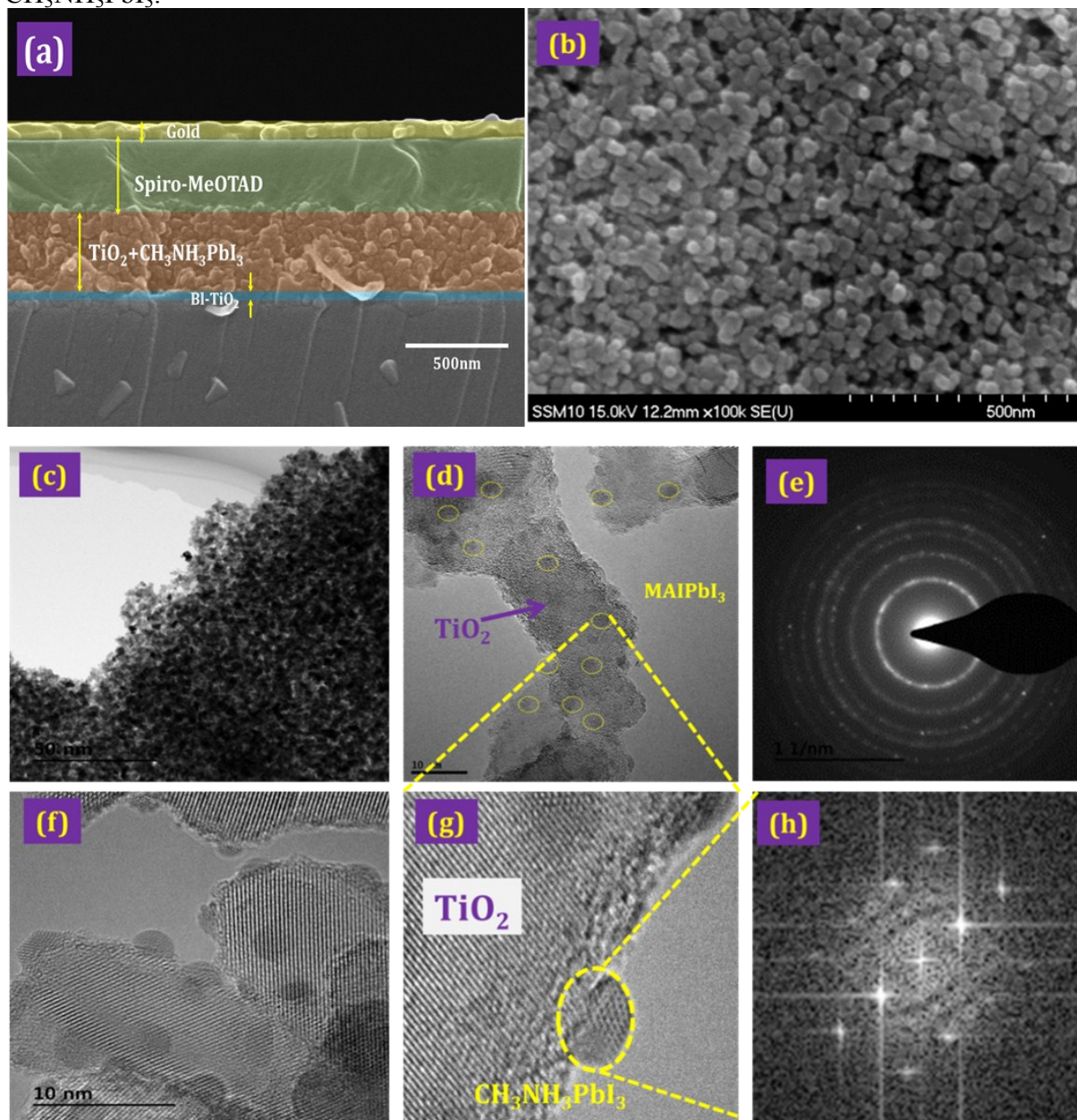


Figure S19 (a) Plan view of TSEM micrographs of P25/CH₃NH₃PbI₃ and EDS mapping of (b) titanium, (c) lead and (d) iodine element.

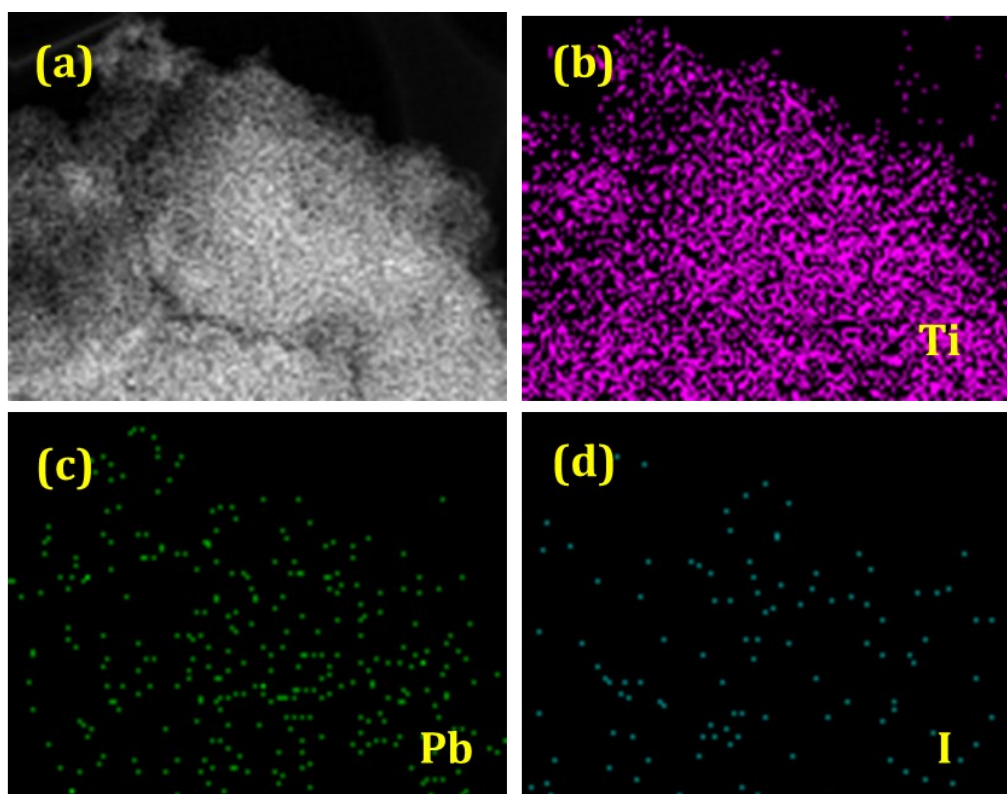


Figure S20 EDS spectrum of selected area of Au@TiO₂ (commercial paste) based perovskite device

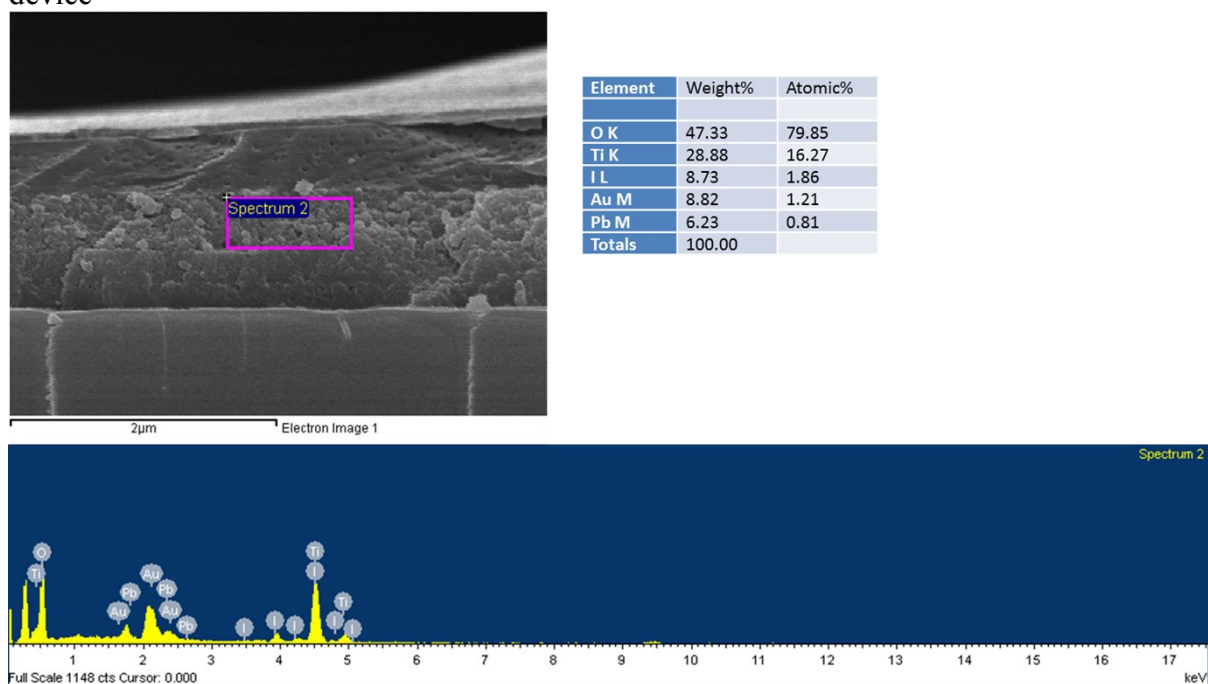


Figure S 21(a) XRD pattern of mp-TiO₂ sample deposited on to glass substrate.

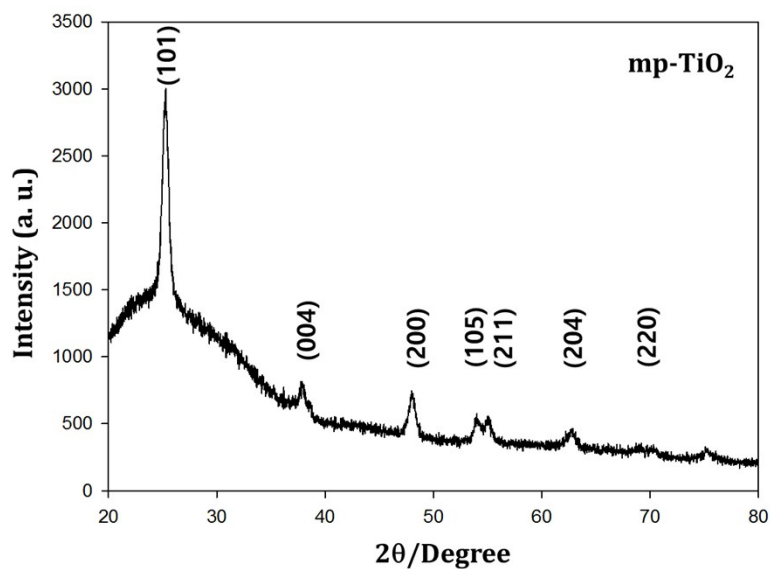


Figure S 21(b) XRD pattern of mp-TiO₂ sample deposited on to FTO substrate. The peaks denoted by star (*) symbol are originated from FTO substrate.

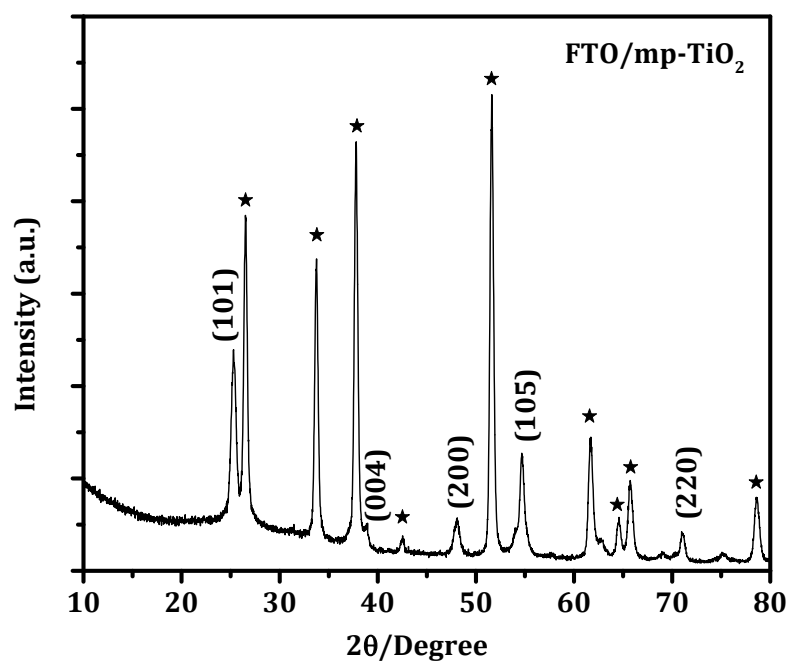


Table S1 Optimization of Spiro-MeOTAD HTM layer and respect to their device performance of bare TiO₂ nanofiber based and Au@TiO₂ nanofiber based devices. Thickness of HTM were optimized by using spin coating rate.

TiO ₂ Nanofibers	Thickness (~nm)	V _{OC} (V)	J _{SC} (mAcm ⁻²)	FF (%)	η (%)	Au@TiO ₂ Nanofibers	V _{OC} (V)	J _{SC} (mAcm ⁻²)	FF (%)	η (%)
Device-A'	450	0.829	19.06	0.44	6.95	Device-A''	0.963	17.51	0.39	6.5
Device-B'	410	0.961	14.57	0.40	5.61	Device-B''	0.951	19.18	0.50	9.12
Device-C'	380	0.869	16.23	0.52	7.19	Device-C''	0.949	19.94	0.53	10.03
Device-D'	366	0.967	16.72	0.51	8.08	Device-D''	0.954	19.22	0.56	10.26
Device-E'	315	0.860	14.23	0.61	7.47	Device-E''	0.952	21.58	0.63	12.94
Optimized	280	0.953	19.52	0.60	11.16	Optimized	0.986	21.63	0.70	14.92